E. coli Superdiffusion and Chemotaxis—Search Strategy, Precision, and Motility

F. Matthäus,[†*] M. Jagodič,[‡] and J. Dobnikar[§]
[†]Center for Modeling and Simulation in the Biosciences (BIOMS), University of Heidelberg, Heidelberg, Germany; [‡]Institute of Mathematics, Physics and Mechanics, Ljubljana, Slovenia; and [§]Department of Theoretical Physics, Jožef Stefan Institute, Ljubljana, Slovenia, and Department of Chemistry, University of Cambridge, United Kingdom

ABSTRACT *Escherichia coli* motion is characterized by a sequence of consecutive tumble-and-swim events. In the absence of chemical gradients, the length of individual swims is commonly believed to be distributed exponentially. However, recently there has been experimental indication that the swim-length distribution has the form of a power-law, suggesting that bacteria might perform superdiffusive Lévy-walk motion. In *E. coli,* the power-law behavior can be induced through stochastic fluctuations in the level of CheR, one of the key enzymes in the chemotaxis signal transmission pathway. We use a mathematical model of the chemotaxis signaling pathway to study the influence of these fluctuations on the *E. coli* behavior in the absence and presence of chemical gradients. We find that the population with fluctuating CheR performs Lévy-walks in the absence of chemoattractants, and therefore might have an advantage in environments where nutrients are sparse. The more efficient search strategy in sparse environments is accompanied by a generally larger motility, also in the presence of chemoattractants. The tradeoff of this strategy is a reduced precision in sensing and following gradients, as well as a slower adaptation to absolute chemoattractant levels.

INTRODUCTION

Living matter is highly imperfect, due to its dynamically changing composition and fluctuating environment. However, despite this fact, many biochemical networks work with a fascinating precision. A good example is the bacterium *Escherichia coli*. Being too small to sense the nutrient gradient along the side of its body (i.e., the cell membrane), *E. coli*, to survive, searches for nutrients in space by maintaining a remarkable system of biochemical reactions inside the cell, called the chemotaxis-signaling pathway. Chemotaxis allows each bacterium to move toward the nutrient and to avoid poisonous substances with great precision, and it is robust against external and internal fluctuations.

Bacterial chemotaxis of *E. coli* is one of the most studied biochemical networks in nature. Most of the relevant proteins involved, and their interactions, have been identified. Furthermore, the chemotactic reaction network inside the cell is one of the few biochemical networks that is well isolated from the rest of the metabolic reactions making chemotaxis a suitable biological system for physical modeling. The bacterial chemotactic network consists of the receptors, the signaling pathway, and the flagellar motors. The bacterium *E. coli* typically has 4–6 flagellar motors attached to its cell membrane. The rotation of the flagella drives the motion of *E. coli* in a rather curious way. When all the motors rotate in the counterclockwise (CCW) direction, the flagella form a coherent bundle and the bacterium swims in a straight line. When one or more of the motors rotate in the clockwise (CW) direction, the flagellar bundle disassembles and the cell tumbles, i.e., rotates randomly without moving. Through switching between CW and CCW rotation, *E. coli* can influence their overall direction of motion, for instance to swim toward a source of nutrients. The sensing of a chemical gradient and its influence on the tumbling probability is regulated through the chemotaxis signaling pathway, a cascade of enzyme-catalyzed phosphorylation and methylation reactions.

The chemotaxis signaling pathway of *E. coli* has been extensively studied theoretically on various levels of microscopic detail. The first attempt to quantitatively model the chemotaxis signaling pathway was the two-state model by Asakura and Honda (1), which was later extended and improved several times. Recently, a thorough investigation was performed (2) where the optimal reaction network—satisfying the requirements of robustness and adaptivity—has been identified. There have been several attempts to model the chemotactic reactions on the discrete molecular level in a spatially explicit way (3–6).

Bacterial motion in the absence of a chemotactic gradient has commonly been described as a purely diffusive process with an exponential swim-length distribution (7). In recent studies (8,9), however, it has been shown that under certain conditions the distribution of CCW events (e.g., time intervals of CCW rotation) can have the form of a power-law.

Submitted September 29, 2008, and accepted for publication April 28, 2009.

All authors contributed equally to this work.

*Correspondence: franziska.matthaeus@iwr.uni-heidelberg.de

Editor: Edward H. Egelman.

0006-3495/09/08/0946/12

doi: 10.1016/j.bpj.2009.04.065

At a constant speed of the bacteria, a power-law in the time intervals of CCW events leads to a power-law in the swim-length distribution, macroscopically observed as anomalous superdiffusion (10).

One form of superdiffusion, the Lévy-flight, corresponds to an inverse power-law distribution of flight lengths. It has been reported (11–16) to be the optimal strategy for a truly random searcher when food or targets: 1), are randomly distributed; 2), are present at low density; and 3), regenerate after each visit. In our model, the individual bacteria swim with a constant speed, therefore the Lévy-walks rather than Lévy-flights are a relevant superdiffusive behavior. Under similar conditions as 1–3, we expect the Lévy-walks to be an optimal search strategy for a random searcher. A truly random search excludes strategies like sensing, learning, and controlled behavior. Such sophisticated search strategies can often be more efficient in comparison to the diffusive behavior (Brownian motion or Lévy-walks). Benhamou (17), for example, finds that in patchy environments a composite Brownian search strategy with long runs in between patches and short runs within patches is more efficient than Lévy-walks. Thus, a search strategy can be more efficient if the random walker is more intelligent such that it can either choose among a variety of behaviors or is capable of sensing the target (for instance through chemotaxis (18)) or any other feature that makes its behavior less random. In absence of chemical gradients (hence the absence of chemotaxis), *E. coli* bacteria perform a true random search without interaction with the environment. Under this condition, a Lévy-walk is a more efficient search strategy than classical Brownian motion and might be of advantage in finding nutrients.

The origin of the power-law swim-length distribution can be found in the chemotaxis signaling pathway. In Korobkova et al. (8), it has been shown that fluctuations in the concentration of one key enzyme, CheR, are passed through the network, leading to large variations in the swim-lengths of individual runs.

In this article, we investigate the influence of CheR fluctuations on the chemotactic movement. We quantify the efficiency of chemotactic motion by introducing an appropriate measure (i.e., the success index). In a given nutrient environment, an efficient chemotactic cell will swim along the gradient and stay localized around a peak of the nutrient distribution. The bacteria are described on the level of objects that react to changes in the environment in a complex way, determined by solving a set of equations describing the chemotactic signaling pathway for each single cell. We numerically simulate the motion of large bacterial populations in two dimensions in various nutrient environments and compare the efficiency of chemotaxis of two populations: bacteria with constant CheR concentration, and bacteria with fluctuating CheR concentration.

THE MODEL

We adapt the two-state model of the bacterial chemotactic network first described in Barkai and Leibler (19) and later extended in Kollmann et al. (2). Here, a receptor complex in the *E. coli* membrane can switch between an active and an inactive state. The probability to be in either state depends on the ligand concentration and on the methylation level of the receptor complex. In the active state, CheA (one of the components of the receptor complex) donates phosphate to the response regulator CheY, which, in its phosphorylated form, binds to the flagellar motor and induces tumbling. The receptor can be multiply methylated, with CheR regulating methylation and CheB regulating demethylation. A higher level of methylation increases the probability of the receptor to switch to the active state (i.e., tumbling). The ligand, if it is an attractor as assumed here, binds with higher affinity to inactive, than to active, receptors, thus stabilizing the inactive state. Furthermore, only active receptors are methylated and only inactive receptor complexes are demethylated. The system of phosphorylation and methylation processes is schematically displayed in Fig. 1.

The methylation process is responsible for the capability of bacteria to adapt to a given level of ligand concentration, while preserving their sensitivity to relative concentration changes. In Kollmann et al. (2), a set of models was investigated, varying from the rather simple model of Barkai and Leibler (19) to more complicated models, where various feedback loops were accounted for. For our simulations, we adapt the third model from the set—the simplest model that guarantees sufficient robustness against intercellular variations in protein concentrations. In comparison to the original Barkai-Leibler model, this model involves a feedback regulation of CheA-P on CheB, and an additional enzyme CheZ substituting auto-dephosphorylation of CheY-P. According to Kollmann et al. (2), this model represents the experimentally established chemotaxis-signaling pathway of *E. coli*. The model is given as a system of coupled ordinary differential equations (see Eqs. 6*a*–6*d*), describing the reaction kinetics of the phosphorylation and methylation processes. The system is extended by the motor switching curve, an algebraic equation that returns the probability of tumbling based on the concentration of CheY-P (7). The equations are solved numerically to obtain a time series for the concentration dynamics, and for the run-and-tumble behavior. In contrast to discrete molecular modeling of the reactions, which are computationally expensive, the continuous approach can yield long time solutions in a computationally cheap way. It is therefore the better choice to investigate the long-time behavior of large populations of cells.

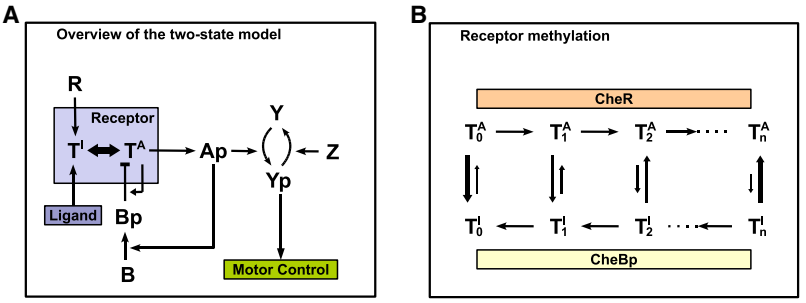

FIGURE 1 Schematic representation of the regulatory processes involved in signal transduction. (*Left*) Overview of the two-state model with all phosphorylation steps. (*Right*) Scheme of the receptor methylation process. The active state of the receptor is denoted by T^A, the inactive state by T^I. The subscript denotes methylation.

CheR fluctuations

Using a stochastic simulation tool (StochSim (20)) in which all molecules are modeled as individual particles, it was shown that a power-law run-length distribution can be obtained when the concentration of CheR is low enough such that stochastic effects become important (8). Here, we use a deterministic description, which leads to exponential run-length distributions for any constant concentration level of CheR. Fluctuations can be introduced by changing the constant CheR to a time-dependent variable. Such stochastic fluctuations can have a number of origins—for instance, noise at the gene expression level, or at the level of binding and dissociation to, and from, the receptor. In Levin (21), gene expression noise of chemotactic proteins has been postulated to be a source of nongenetic individuality of *E. coli*, and its effects on the variability and distribution of adaptation times has been investigated. However, the concentration of CheR in the cell has also been observed to remain constant (V. Sourjik, ZMBH, University of Heidelberg, Heidelberg, Germany, personal communication, 2008), which speaks against fluctuation induced by gene expression noise. We therefore understand the fluctuations of CheR as fluctuations in receptor binding and dissociation processes and not as changes in the overall cellular concentration of CheR. For instance, stochastic effects of binding and dissociation of CheR have been studied in Hansen et al. (22), and binding and dissociation rates have been determined by FRET experiments in Schulmeister et al. (23).

Both assumptions (gene expression noise or stochastic binding and dissociation processes), however, can be used to derive the following equation, which describes stochastic fluctuations of CheR:

$$\frac{dR}{dt} = \beta\eta(t). \qquad (1)$$

Here R denotes the concentration of CheR and $\eta(t)$ represents a stochastic process returning white noise in the form of uniformly distributed random numbers from the interval $[-1, 1]$. The constant parameter β determines the noise variance. A similar approach was chosen in Tu and Grinstein (24) to reproduce the power-spectra of the CW/CCW bias. Since R corresponds to a concentration, we have to guarantee positiveness for the solution of Eq. 1, which we achieve by setting a lower boundary $R \geq 0$ for all t. For symmetry reasons, and to ensure an average $\langle R(t)\rangle_t = R_0$, we also set an upper boundary $R(t) \leq 2R_0$. (Note that the existence of these boundaries also ensures the stationarity of the process. The Wiener process, given by Eq. 1, would otherwise diverge for $t \to \infty$. In the time course we are simulating, with the given parameters, these boundaries are, however, extremely rarely reached, and thus do not affect the dynamics of R notably.)

Integration of white noise yields red (or Brownian) noise characterized by a frequency spectrum $\sim 1/f$ with pronounced low-frequency modes. These are passed through the complex signaling pathway resulting in a power-law distribution of the run lengths over many decades. We simulated sequences of run lengths for different magnitudes of β, and found the power-law run-length distributions only for a certain range of values (here, 10^{-3}–10^{-4}). If β is very large, CheR fluctuates too fast for the system to follow, and the run-length distribution is exponential. If β is very small, the concentration of bound CheR changes only very slowly, and thus can cause variations in the run lengths only over very long timescales. In the derivation of Eq. 1, β is given as $k_{\text{off}}R$, with k_{off} the dissociation constant and R the concentration of bound CheR (both measured in (23)), yielding a magnitude of 10^{-3} for β. In Fig. 2, we show the dynamics of fluctuations in bound CheR that lead to a power-law run-length distribution.

We have carried out a set of simulations to investigate the influence of CheR fluctuations in the presence and the absence of chemoattractant gradients. Apart from being computationally inexpensive, an advantage of our deterministic approach of modeling the chemotactic pathway is that the absolute level of CheR and the type of fluctuation can be chosen independently. This makes it possible to study the influence of fluctuations without changing the average level of CheR. In stochastic simulations, Lévy-walks are obtained as a result of low absolute CheR levels where stochastic effects become important. To remove stochastic effects, the absolute CheR concentration is set higher. Thus, when comparing populations with and without CheR fluctuations, this implies comparing populations that differ in their absolute CheR levels, therefore differing also in their average run lengths (see Fig. 3), or in the diffusion coefficient. With the approach presented here, this problem does not occur.

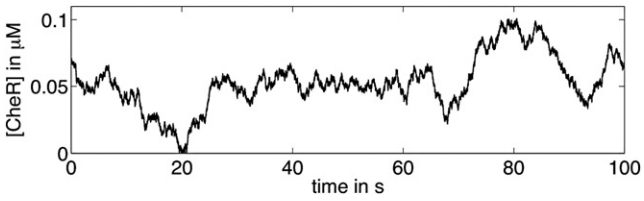

FIGURE 2 CheR fluctuations. The fluctuation of CheR, representing stochastic effects of receptor binding and dissociation, is modeled by Eq. 1. The low-frequency modes of the noise are passed through the signaling pathway, leading to power-law behavior in the run-length distribution.

RESULTS

Run-length statistics

To explore the effect of the fluctuations we introduced in Eq. 1, we first study the motion of bacteria in an environment without nutrients. We compare the motion of bacteria of type A (noise-free network) and type B (noise added to the CheR level). By solving the differential equations (Eqs. 6*a*–6*d*) with Eq. 7, we generate a sequence of run-and-tumble events. Once a bacterium starts to swim, we count the number of consecutive swims to obtain the length of the straight line—the run length. Every straight run is followed by tumbling in which the bacterium changes its orientation

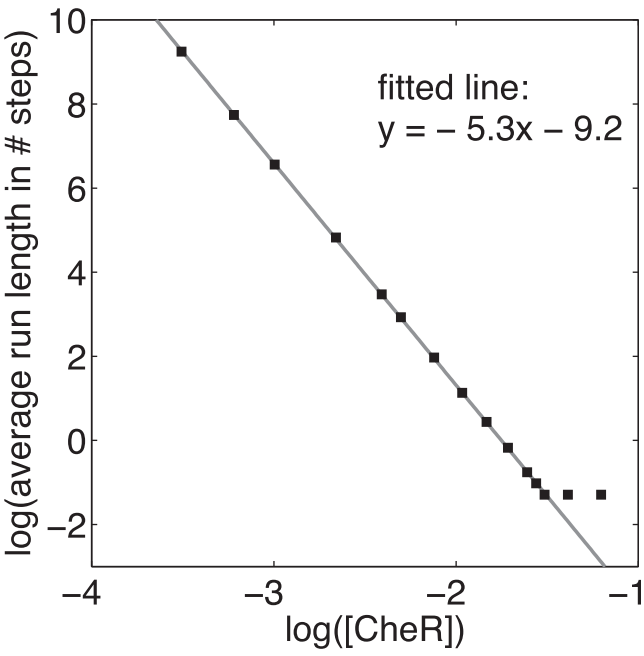

FIGURE 3 Run-length statistics for a constant CheR concentration. Average run length depending on the CheR concentration. The average run length increases for decreasing CheR concentration and vice versa.

without changing its position. Then a new run starts, and so on. We compare the distribution of the run lengths for both types of bacteria. For type A, the distribution is exponential, independent of the CheR level. The level of CheR, however, influences the average run-length—the lower the CheR concentration, the longer the average run-length (see Fig. 3).

For bacteria of type B, a power-law run-length distribution is observed at a sufficiently low average CheR concentration (see Fig. 4). This result is in agreement with the result observed in Korobkova et al. (8), where a power-law distribution of the CCW events was found in stochastic simulations of CheR binding. Also in these simulations, the power-law behavior vanished for an increased CheR concentration. We want to stress that the presences of strong low-frequency modes in the CheR fluctuations is essential to reproduce the power-law statistics. We introduced the slow modes by integrating the white noise in Eq. 1. The slow fluctuations are passed through the signaling pathway, influencing the methylation level and therefore the tumbling probability. If the fluctuations are too fast (for instance, white noise), the run-length distribution would be, again, exponential. Additionally, if the average CheR concentration is too high, the effect of added noise vanishes and the distribution is again exponential. The power-law run-length distribution can therefore be observed only at low CheR levels and low-frequency colored noise. Example trajectories for type A and type B bacteria are shown in Fig. 5, demonstrating typical diffusionlike behavior of the individual A with a constant CheR concentration, and a characteristic Lévy-walk trajectory for bacteria of type B with CheR fluctuating.

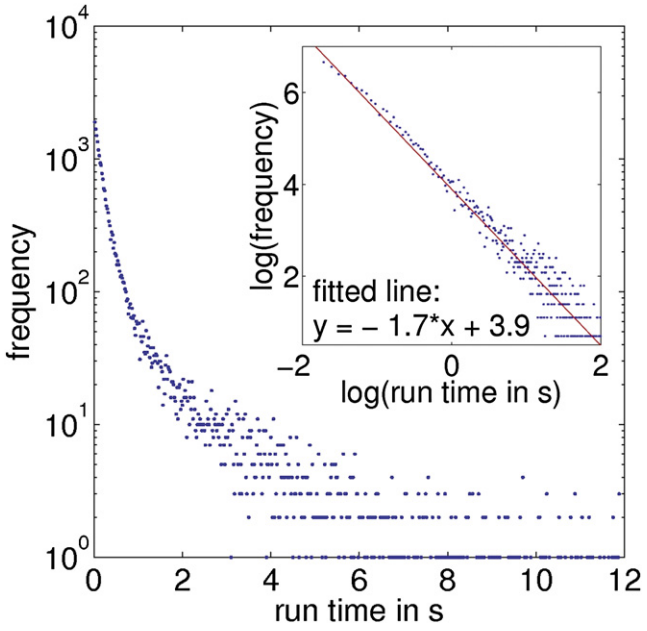

FIGURE 4 Run-length statistics for fluctuating CheR concentration. The run-length distribution gets a power-law tail if the CheR concentration is low and noisy. The inset shows the cumulative of the run-length distribution on double-logarithmic axes.

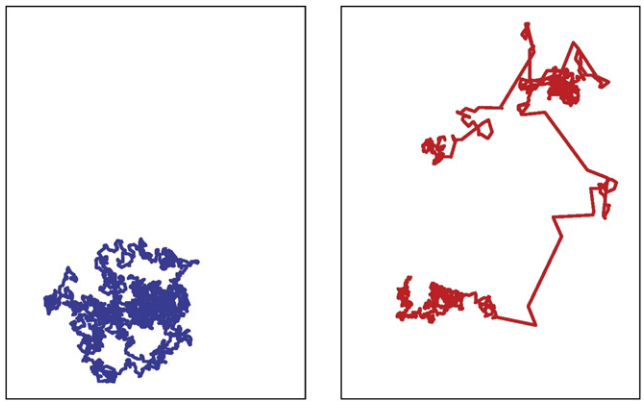

FIGURE 5 Trajectories in a two-dimensional domain. Example trajectories of a bacterium with constant (*left*, online: *blue*. print: *solid/black*) and with fluctuating CheR concentration (*right*, online: *red*. print: *shaded/gray*) in a two-dimensional domain.

Characteristic for a Lévy-walk is the switching between local search and long space-covering walks.

This motion often represents an efficient search strategy, since it gives a very low probability that the random walker returns to a place where it searched before.

Correlation of run lengths

The low-frequency modes in the CheR fluctuations lead to slow changes in the concentration levels of the active and passive form of the receptor, and therefore to slow changes in the probability of tumbling. In periods where CheR is decreasing or low, the run lengths are, on average, longer than at periods in which CheR is increasing or high. Because the changes in the concentration levels are slow in comparison to the duration of a single run, the length of consecutive runs is correlated. In Fig. 6, we show a sequence of run lengths that clearly display characteristic periods of shorter and longer runs.

The success index

Our next numerical experiment involves bacteria of type A and B in various types of nutrient environments. For this we devised a number of simulations with different two-dimensional chemoattractant landscapes and explored how well both types of bacteria perform in each of them. To evaluate how effective the bacteria of different chemotactic strategies are in different environments, we first define a measure θ for the success index, based on the average ligand concentration that the bacteria in the population sense. We assume that the bacteria in an optimally fit population will move in such a way that they will spend most of the time at the position with maximum ligand concentration. For each bacteria i we take its position $\vec{r}_i = (x_i, y_i)$, and compute the ligand concentration at this position $L(\vec{r}_i)$. The success index θ of the whole population is then given as the average,

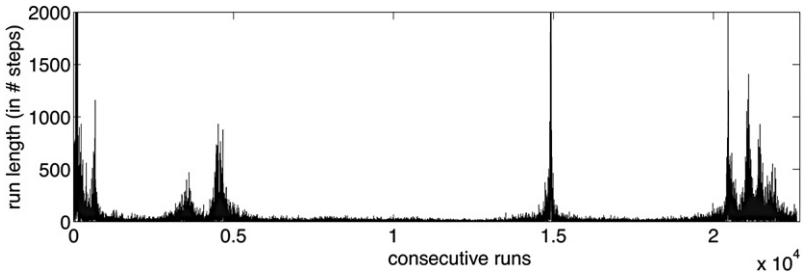

FIGURE 6 Lengths of consecutive runs. Due to the fluctuations in CheR, there are periods with longer, and periods with shorter, run lengths.

$$\theta = \langle L(\vec{r}_i) \rangle. \quad (2)$$

For a given situation (ligand distribution), the change of θ in time can be used to compare the success of the two populations. One population is designated more successful than the other, if it has a higher value of θ. The so-defined success index depends on the environment and is only useful for relative comparison of different populations in the environment with the same nutrient distribution. In the following, we report on the results for three different food landscapes.

Linear gradient

In the first experiment, we study the behavior of both populations in the presence of a linear gradient of the chemoattractant $L(x, y)$ on one-half of the domain. We define

$$L(x,y) = \begin{cases} kx & \text{for} \quad x \geq 0, \\ 0 & \text{otherwise.} \end{cases} \quad (3)$$

Here, k is a parameter defining the steepness of the gradient. The initial position of the bacteria is at the origin ($x = 0$, $y = 0$). The optimal strategy in this situation would be to move straight in positive x direction. Therefore, we measure the success of a population through the average x position of all individuals. In Fig. 7, we show the average x position as a function of time for different gradients.

Generally, the steeper the gradient, the faster the drift of both populations, but the center of mass of population B moves, in the long run, faster up the gradient than the center of mass of population A (constant CheR). The reasons for this are the faster dispersal of the species B on one hand and its impaired adaptation on the other. The latter is seen clearly in the simulation with large k. Here, A adapts quickly to the absolute concentration level (seen as a change in the slope of the curve in Fig. 7), whereas the adaptation of the individuals B with CheR fluctuating is much slower.

In Fig. 8, we show snapshots of the distribution of the bacteria at $t = 500$ s for the different gradients. It is evident that the two populations differ not only in the speed of their drift, but also in the response of their individuals to the gradient. Whereas population A behaves as a bulk, where all individuals respond very similarly to the gradient, there is a large variation in the behavior of population B. For every gradient, there is clearly a subpopulation of B that has moved far more to the right than any of the individuals with constant CheR. However, there is also a large subpopulation of B that moves much slower than the average of A, and there is a nonnegligible part of the population B that moved far away in the wrong direction.

Summarizing, these simulations show that CheR fluctuations enhance the variability of the behavior of a population, but at the cost of a deficient adaptation. In population B, the success of individuals depends greatly on their good or bad luck. In our experiment, individuals are ''lucky'' if their level of CheR is decreasing or low, and if they happen to hit the proper direction; in this case, they do long runs in the proper direction, and move much further to the right than any individual of A. Individuals of type B can be ''unlucky'' either by being in a state of doing long runs in the wrong direction or by being in a phase where CheR is increasing or high, in which case the step lengths are short, and the individuals tumble around the starting position.

Trapezoid barrier

Individuals that, due to CheR fluctuations, are in a period of doing longer run lengths can move much faster up a ligand gradient than individuals with CheR constant. If, however, the ligand concentration decreases after some point, then the same individuals that before profited from their long run lengths might now be too fast to respond to the change in the ligand concentration, and to correct their direction.

The second experiment is therefore designed to compare the chemotactic precision of the two populations, whereby we understand precision as the ability to find a maximum of the ligand concentration and stay there. For this, we define the ligand concentration as

$$L(x,y) = \begin{cases} k_1 x & \text{for} \quad 0 < x \leq x_1 \\ L_m & \text{for} \quad x_1 < x \leq x_2 \\ L_m - k_2 x & \text{for} \quad x_2 \leq x < x_3 \\ 0 & \text{for} \quad x \leq 0, x > x_3 \end{cases}. \quad (4)$$

Here k_i, L_m, and x_i are positive constants, with $0 < x_1 < x_2 < x_3$. The ligand concentration landscape $L(x, y)$ resembles a linear barrier with a flat top (see Fig. 9). We again choose the origin as starting position for all individuals.

In Fig. 10, we show snapshots of bacterial positions at different time steps. The figure shows only a small region of the space, close to the area where the ligand is present. The snapshots show that both populations behave similarly.

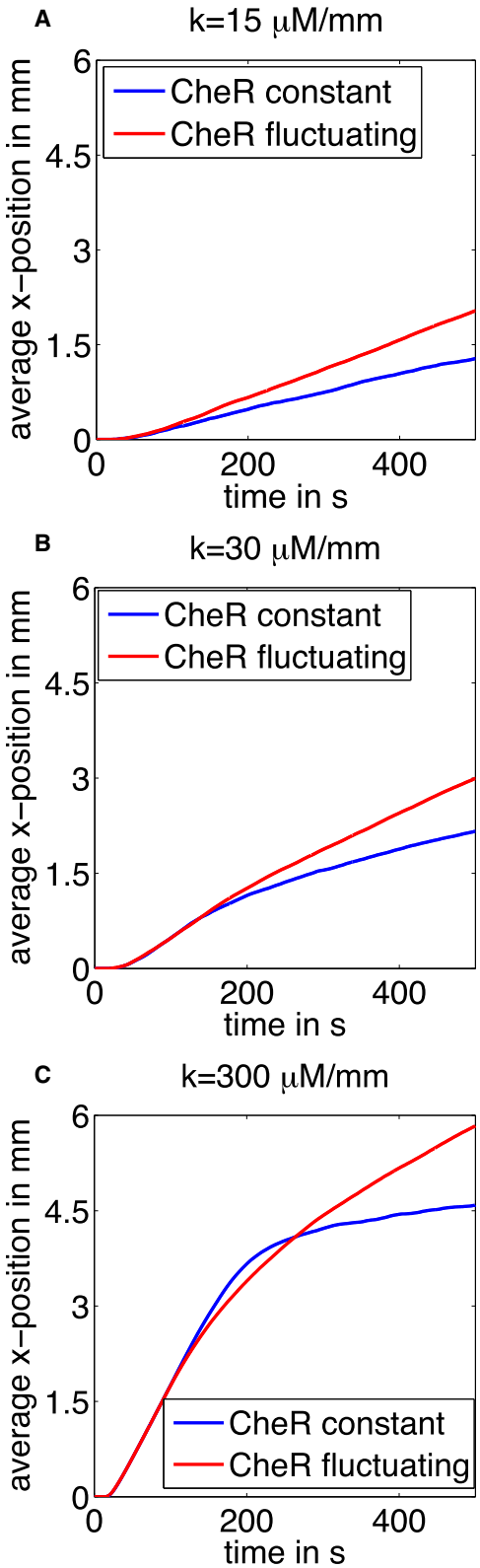

FIGURE 7 Average x position as a function of time. The larger the gradient of the ligand, the stronger the drift of the populations. In the long run, population B with CheR fluctuating (*red*, *solid line*) has its center of mass at a position with higher ligand concentration. The change in the slope of the black dashed curve is a sign that population A (*blue*, *dashed line*) adapts to the absolute ligand concentration. The fact that the change in the slope is much less pronounced in the gray solid curve indicates an impaired adaptation of population B.

First, the bacteria move in the direction of increasing concentration. This is followed by an overshooting, in which a large part of the population hits the area where the gradient decreases. Individuals change direction, return to the area of maximal ligand concentration, and then disperse in y direction only. This experiment is very well suited to show the differences in the precision of the two populations. For population type A, the area with $L = L_m$ acts like a trap; no single individual crosses this stripe to end up on the right-hand side of it. In contrast, there are individuals of type B with fluctuating CheR, which might do a long run and end up at a position $x > x_3$. Whether this is good or bad luck depends, of course, on the presence or absence of a chemoattractant in the domain with $x > x_3$.

In Fig. 11, we show the distribution for both populations in the entire domain. The striking difference is that most of the individuals A accumulate at high ligand concentration, whereas many individuals of type B get lost at either side of the trapezoid. In Fig. 12, we show the time course of the success index θ. The initial oscillation in the curve is a consequence of the overshooting of the bacteria into the area of decreasing ligand, and their subsequent return to the area of high ligand concentration. All individuals A stay afterwards at positions of high ligand concentration. In contrast, the success index of population B decreases in time, as individuals stray from the area of high ligand concentration.

This experiment shows that both populations differ in their chemotactic precision. The higher variability in the run lengths of B and the impaired adaptation lead to a decreased precision and the inability of individuals to stay in areas of maximal ligand concentration.

Multiple Gauss peaks

The third and last experiment is designed to test both populations in an environment in which the ligand distribution is sparse, and individuals have to search for it. In particular, we model the ligand distribution as a set of Gaussian peaks randomly distributed in the domain. The peaks differ in their height and width. The initial position is again the origin. Also in this experiment, the population B disperses much faster than A, due to some individuals with larger run lengths that reach the Gaussian ligand peaks first (see the first peak in the success index of B, shown in Fig. 13). In Fig. 14, we show the distribution of both populations at the end of the simulation. One can see that population B, performing a Lévy-walk, actually found all ligand peaks. However, because these individuals switch between phases of longer and shorter run lengths, they often stray away from the peaks they have already found and have to start searching again. The overall number of individuals at positions of high ligand concentration is therefore lower than in population A, which

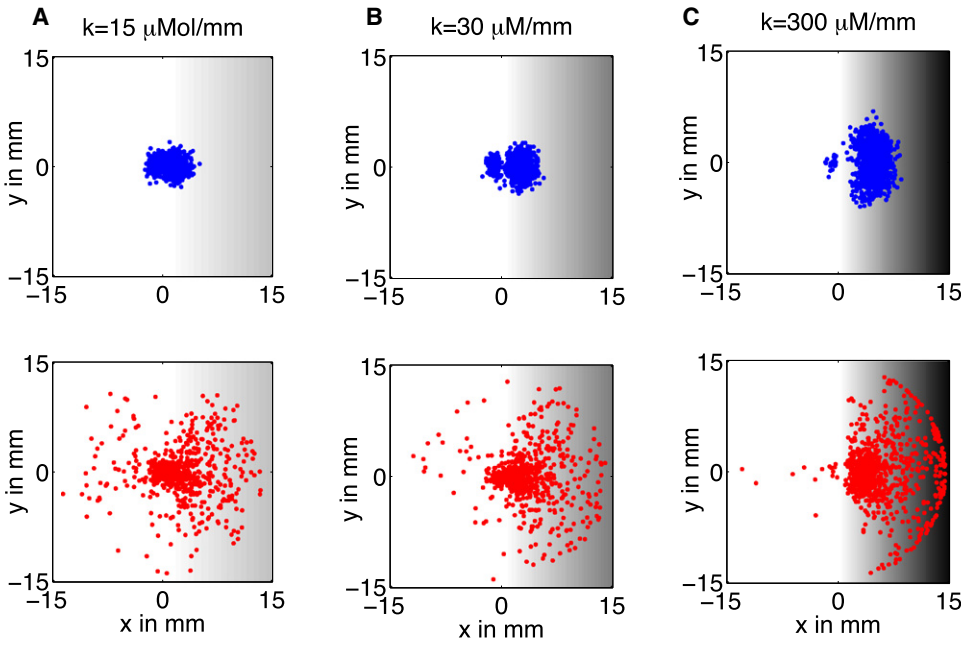

FIGURE 8 Bacterial positions at the end of the simulation, superimposed on the ligand concentration. The distribution of bacteria at the end of the simulation shows that population B (fluctuating CheR concentration, shown in *red squares* in the *lower row*) is characterized by a larger behavioral variability, and a larger motility of some individuals. In contrast, population A (constant CheR, shown as *solid blue circles* in the *upper row*) displays a stronger bulk behavior and lower motility.

disperses much slower. At the same time there is a notable accumulation of individuals in only two out of the five peaks. However, individuals that have found one of the peaks also stay at the peak with very high probability. Hence, this is yet another experiment showing that CheR fluctuations increase motility but reduce chemotactic precision.

DISCUSSION

More and more animal species have been reported to perform search strategies characterized by power-law run- or flight-length distributions, ranging from marine predators (26) such as the albatross (15), to spider monkeys (27) and to humans (28,29) (see also the collection of references in (17)). However, there are also reports showing that some of those measurements are either erroneous or that the measured distribution appears as a power-law on the log-log plot, but more sophisticated methods reveal that the distribution is not genuinely power-law (30–32). Another issue is that the Lévy-distribution in the run or flight lengths might originate from the interaction with the environment, such as in the case of the spider monkeys, where it seems to be related to a power-law distribution of tree sizes (33). The question therefore is whether, in the case of *E. coli*, the power-law is real, and how it is generated.

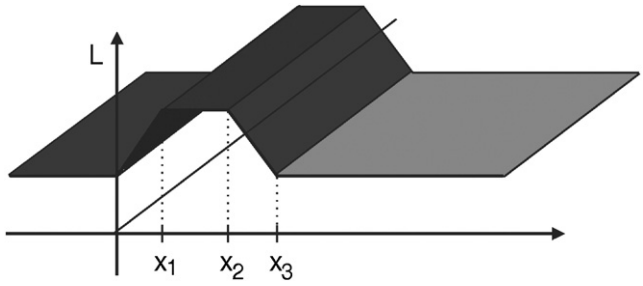

FIGURE 9 Illustration of the trapezoid ligand distribution. The ligand distribution illustrated here is defined in Eq. 4.

There are experimental as well as simulation results supporting the existence of Lévy-walks for which the power-law distribution of the run lengths extends over many magnitudes. On the experimental side, there is the finding of Korobkova et al. (8) reporting a power-law in the CCW events over many scales. In support of these experimental findings, the stochastic simulation tool StochSim (20) was used to show that stochastic effects in the case of low levels of CheR can indeed induce power-law run length distributions. We used a modified approach, combining a deterministic model with stochastic input in the variable CheR and also obtain power-law run-length distributions for a wide range of parameter values. The power-law is genuine and persists if, instead of the log-log plot, the cumulative (survival) distribution is plotted (not shown).

A good argument speaking in favor of a power-law run-length distribution is the following: If a Lévy-walk does present an evolutionary advantage for *E. coli* in some situation, and if the chemotaxis signaling pathway allows this kind of variability in the run lengths (for instance, through stochastic fluctuations of one of its enzymes), then it is very likely that at least some subpopulation of *E. coli* does indeed perform Lévy-walks. We used our mathematical model to address precisely the last two points. First, we confirm that the chemotaxis-signaling pathway does allow a power-law run-length distribution; second, we try to evaluate in which situations and aspects the power-law run-length distribution presents an advantage and when not. The fact

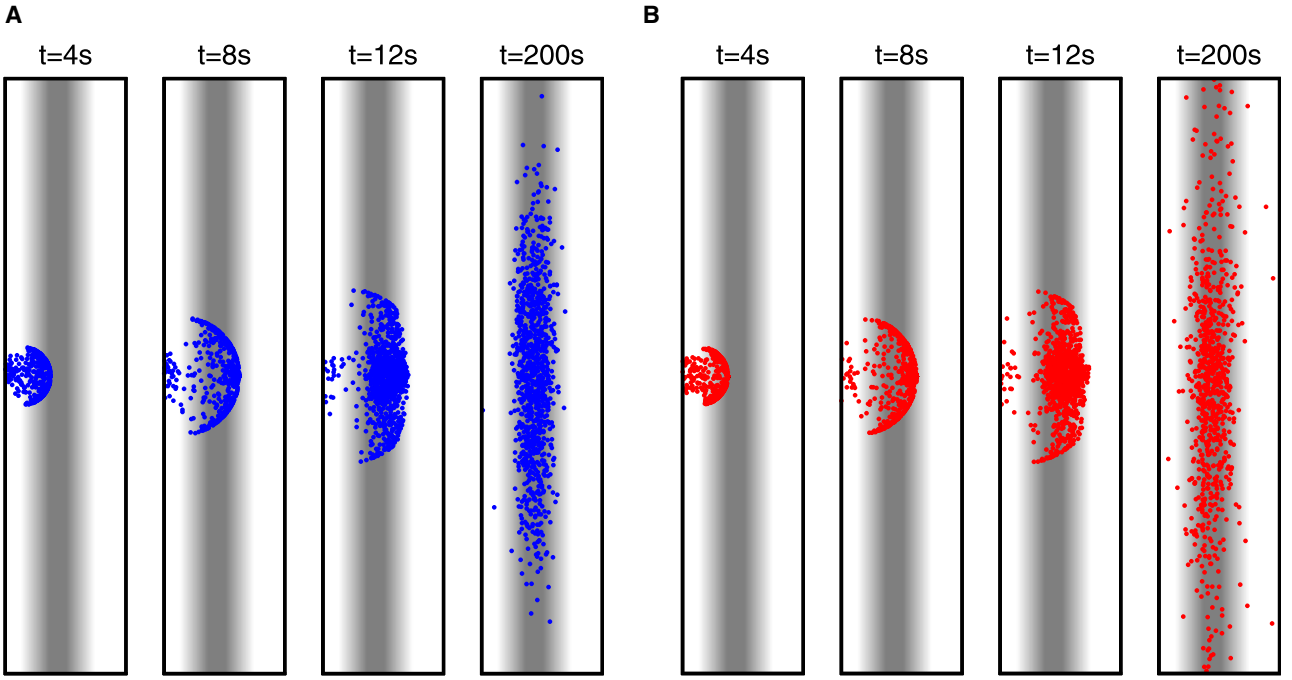

FIGURE 10 Snapshots of bacterial positions in the vicinity of the trapezoidal barrier at different time steps. Population A is illustrated on the left (*blue circles*), population B on the right (*red squares*). Both populations first move up the gradient, overshoot the area where the ligand has the maximal concentration, return, and then disperse in the area with maximum L.

that we find situations in which the population performing a Lévy-walk is more efficient speaks in favor of the Lévy-walk—but as this is a result of mathematical modeling, it is not a proof of its existence in nature.

Another very interesting question is how the stochastic fluctuations in CheR actually induce power-laws in the run-length distribution. Our observation is that the appearance of the power-law distribution depends on the return-time statistics of the bounded Brownian noise model for CheR fluctuations. We find that the power-law extends over many scales for values of the parameter β in a certain interval. For smaller values of β, the time variation of CheR is very slow and the power-law statistics is not observed within the limited simulation time. For larger β, the bounded Brownian noise is characterized by shorter return times and the run-length distribution by a truncation in the power-law. The fluctuations in the CheR level are passed through the complex chemotactic-signaling pathway, and the concentrations of the other enzymes involved are never at a steady state. However, if the fluctuations in CheR are characterized by long return times, the level of CheR stays above or below the average value long enough for the rest of the pathway to follow this change. In this way the tumbling frequencies can grow both very high and very low, and therefore cover a much wider range. For fast variations characterized by short return times, the typical response of the system is too slow, and variations in the tumbling frequency are smaller; therefore the power-law becomes truncated.

Any constant CheR concentration leads to an exponential run-length distribution, whereby the average run length depends on the CheR concentration in a nonlinear way (it

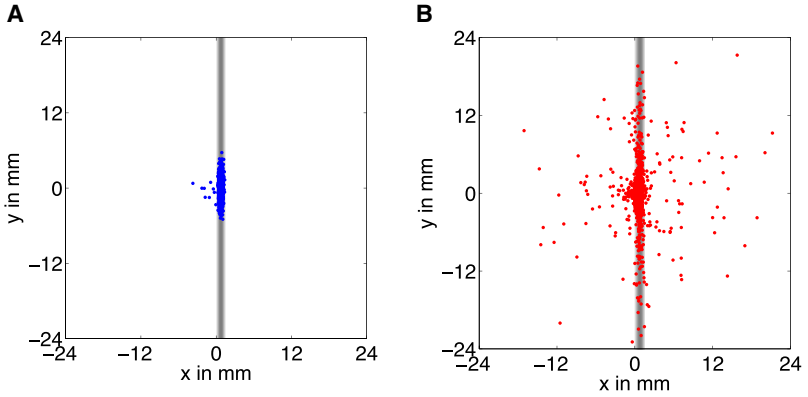

FIGURE 11 Bacterial positions at the end of the simulation, superimposed on the ligand concentration (trapezoidal barrier). The figure shows that almost all individuals of population A (*blue circles*, *left*) are located in the area with large ligand concentration. No single individual moved across the barrier to the right side of the domain. Some individuals of population B (*red squares*, *right*), in contrast, crossed the barrier. This indicates a larger chemotactic precision of population A.

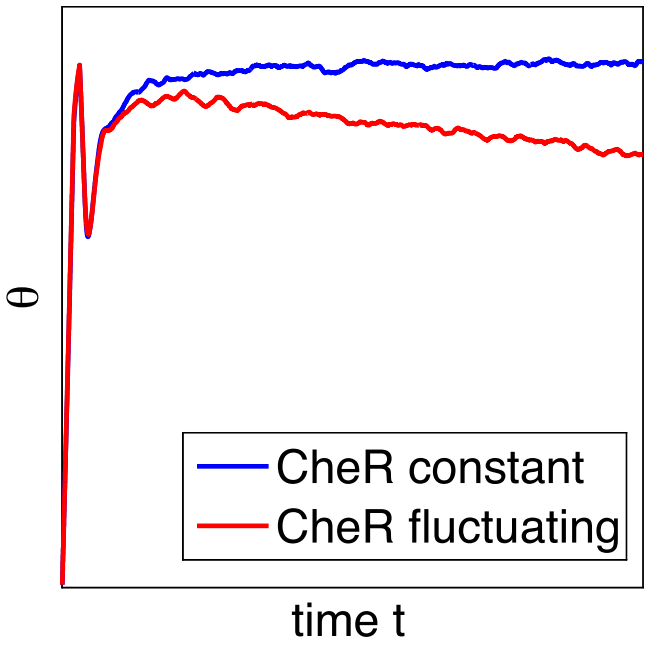

FIGURE 12 Success index for both populations moving in the domain with trapezoid ligand distribution. The initial oscillation is due to the overshooting of both populations. In the long term, the population with CheR constant (*blue*, *dashed*) stays precisely in the area with high ligand concentration, whereas individuals of the population with CheR fluctuating (*red*, *solid*) become lost to either side, and move away.

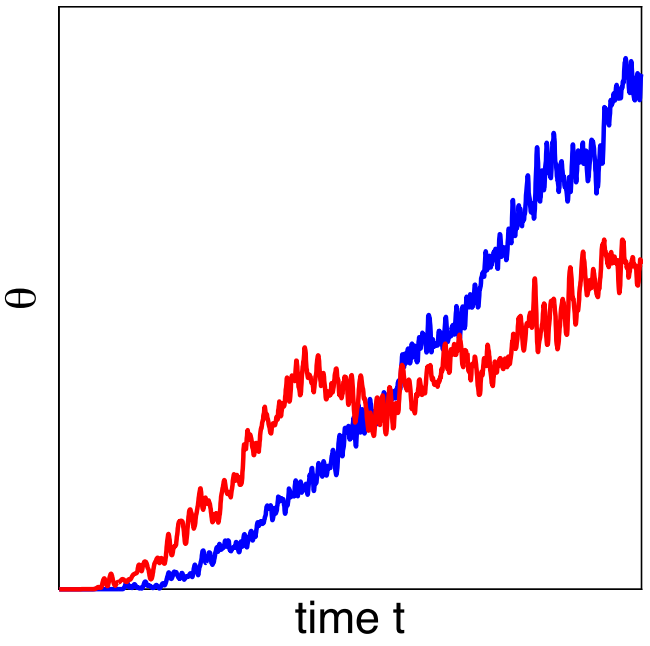

FIGURE 13 Success index for the two strategies in the environment with several sparse nutrient sources. In the long run, population A (*blue*, *solid*) is more successful due to its larger chemotactic precision. In the short run, however, population B (*red*, *shaded*) has, on average, more access to the chemoattractant due to the fraction of individuals with very large motility.

has the form of a power-law; see Fig. 3). When the CheR concentration varies with time, the time-averaged distribution of the run lengths can be thought of as a superposition of many exponential distributions with various average run lengths. As shown in Mommer and Lebiedz (34), a superposition of exponential distributions with proper weights can yield a (transient) power-law distribution. To illustrate this, we have performed several separate simulations with time-independent CheR concentrations covering a certain interval. Each individual run is characterized by an exponential distribution, but the superimposed run-length distribution is power-law over many scales. From our simulations with fluctuating CheR concentrations, it is evident that a bounded Brownian noise model also meets the requirements in Mommer and Lebiedz (34), and leads to the power-law behavior for biologically reasonable values of the model parameters. We have also replaced the Brownian noise by an Ornstein-Uhlenbeck process, given as $dR(t) = [K(R^* - R) + \beta\eta(t)]dt$, where R^* denotes the long time expectation of $R(t)$, and K and β are parameters. In addition, for the Ornstein-Uhlenbeck process we have found power-law run-length distributions for a wide range of parameters (data not shown), thus the model is robust in this aspect.

Note that, from the above discussion, we can conclude that the real source of the power-law behavior is the nonlinearity of the reaction network (*curve* in Fig. 3), whereas the input CheR variations must provide a proper sampling within an interval on this curve. It is tempting to speculate that—at given fixed kinetic constants characterizing the network (see Table 1)—the observed power-law exponents should be more or less universal. However, we did not perform a thorough statistical analysis to support this idea.

Bounded Brownian noise and the Ornstein-Uhlenbeck process both feature exponential asymptotic distribution of return times. Therefore, the power-law run-length distribution is truncated. The Lévy-walk resulting from a truncated power-law run-length distribution has identical properties to real Lévy-walks, but is a transient phenomenon and a crossover to classical diffusion occurs for large enough times. In our simulations and for the chosen parameter of β the truncation is not observed, but long runs are rare and do not allow a good statistics on this issue. In the real system, an important timescale is the life span of *E. coli*, and even if the Lévy-walk is a transient phenomenon, it might be very relevant for the bacteria if the crossover time is of similar order.

In earlier studies it has been shown that the run-length distribution of *E. coli* can have the form of a power-law, induced by stochastic fluctuations of CheR, one of the key enzymes of the chemotaxis-signaling pathway. This type of run-length distribution might be of evolutionary advantage, since the resulting Lévy-walk represents an advantageous search strategy in environments with sparse nutrient distribution. The fluctuating enzyme, however, fulfills an important role in the chemotaxis-signaling cascade. It controls the methylation level of the receptor, and therefore the adaptation to the absolute ligand concentration. If the

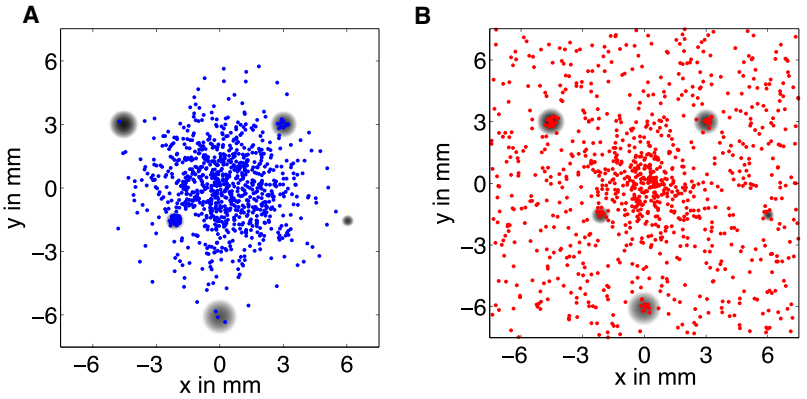

FIGURE 14 Bacterial positions at the end of the simulation, superimposed on the sparse ligand concentration. Population B (*right*, *red squares*), characterized by a larger motility of some of the individuals, has covered the entire area and found all the nutrient sources. Population A (*left*, *blue circles*) dispersed more slowly, and in the same time, found only three of the peaks. Note that individuals that have localized around a peak have a larger probability to stay there than individuals of population B.

adaptation is not fine-tuned, then the sensitivity to gradients is affected. Hence, it is to be expected that CheR fluctuations might be of advantage in absence of chemoattractants, but are disadvantageous when it comes to chemotactic motion.

A recent publication of Emonet and Cluzel (36) studies the relation between adaptation and behavioral variability from a slightly different point of view. In particular, they show that the sigmoid form of the activation curve of the receptor complex with respect to CheR has an influence on both adaptation and noise amplification. Their article nicely complements our findings presented here. In Emonet and Cluzel (36), the influence of the steepness of the activation curve on adaptation and noise amplification is studied, while we keep the activation curve constant and investigate the influence of the noise itself on adaptation and sensitivity.

CONCLUSIONS

In this study we have explored how stochastic variations in the CheR level combined with a deterministic model of the chemotactic-signaling pathway in *E. coli* leads to the superdiffusive behavior of the bacteria in a solution without chemoattractants. One of the key findings of our study is that CheR fluctuations induce a large variability in the behavior of individuals. At every point in time, there are individuals characterized by a very high motility, whereas many others have a very low motility. The individuals with larger average run lengths are able to move very fast up the gradient, but are at risk to accidentally move far away from the area in which the ligand concentration is high. Individuals with short run lengths are more precise, but slower.

If we would compare the two populations in a more realistic experiment we would put them both in the domain and include two effects in our simulation: ligand consumption and bacterial reproduction. In direct competition of populations A and B, behavioral variability of type B is expected to be of advantage, especially in environments with sparse and short-lived gradients. The fast individuals would find the food first, eat it, reproduce, and go on searching, whereas the slow and precise type A bacteria might find themselves trapped in a large area of no food and die. However, the ranking of the strategies clearly depends on the environmental conditions. In an environment with steep and stable gradients, population A would prevail. Another feature of population A with a constant CheR level is its bulklike behavior, which should present a disadvantage if the chemoattractant turns out harmful for the bacteria. Since all individuals respond with similar intensity, the damage would affect all of them. A large variability in the chemotactic response in the case of fluctuating CheR in type B would expose only a fraction of the population to the toxin, whereas the rest would survive.

Summarizing, fluctuations lead to a higher variability in the run lengths and to variability in the response to chemical gradients. Adaptation and chemotactic precision are impaired, but the higher variability in the behavior is, in some cases, still advantageous for the population. If the chemoattractant represents nutrition, then individuals that find it first, profit. If the chemoattractant turns out harmful, the population might survive because of ''unlucky'' individuals that quickly move away from the gradient. And finally, the different motilities lead to faster dispersal and therefore reduced interspecies competition.

APPENDIX

The mathematical model of the chemotaxis-signaling pathway

The model of the chemotaxis-signaling pathway used in this article is the same as model 1*c* presented in Kollmann et al. (2). For readability of this article, the equations and parameter values are summarized below.

For a given ligand concentration L, the probability of the (m-times methylated) receptor complex T_m to be in the active state is given by

$$p_m(L) = V_m\left(1 - \frac{L^{H_m}}{L^{H_m} + K_m^{H_m}}\right). \tag{5}$$

The system of equations describing the concentration dynamics involved in the chemotaxis signaling pathway (see (2)) are given below:

$$\frac{dT_m}{dt} = k_R R\frac{T_{m-1}}{K_R + T^T} + k_B B_p\frac{T^A_{m+1}}{K_B + T_A} - k_R R\frac{T_m}{K_R + T^T} \tag{6a}$$

$$-k_B B_p \frac{T_m^A}{K_B + T_A},$$

$$\frac{dA_p}{dt} = k_A\left(A^T - A_p\right)T_A - k_Y A_p\left(Y^T - Y_p\right) - k_B'A_p\left(B^T - B_p\right), \quad (6b)$$

$$\frac{dY_p}{dt} = k_Y A_p\left(Y^T - Y_p\right) - k_Z Y_p Z - \gamma_Z Y_p, \quad (6c)$$

$$\frac{dB_p}{dt} = k_B'A_p\left(B^T - B_p\right) - \gamma_B B_p. \quad (6d)$$

In this system of equations, T_m denotes the m-times methylated receptor complex, and $T_A = \sum_m T_m^A$ the concentration of active receptor complexes, whereby, $T_m{}^A = p_m(L)T_m$. By A^T, we denote the total concentration of CheA with A_p, the concentration of CheA in its phosphorylated form, CheA-P. Similarly we denote the concentration of phosphorylated forms of CheB and CheY by B_p and Y_p, and the total concentration by the superscript T. R stands for the concentration of CheR, and Z for the concentration of CheZ. The constants k^* and γ^* represent kinetic rates, and Michaelis-Menten constants are named K^*.

These equations, describing the concentration kinetics of all signaling molecules involved in the chemotaxis signaling pathway, are complemented by the motor switching curve (see Eq. 7). This curve is a relation that defines the probability of tumbling τ for a given concentration of CheY-P, and has been measured in Cluzel et al. (37),

$$\tau = \frac{Y_p^{H_c}}{Y_p^{H_c} + K_c^{H_c}}. \quad (7)$$

The parameters used for our simulations are given in Table 1.

TABLE 1 Parameter values used in the simulations

Constants		
k_R	0.39 s^{-1}	
k_B	6.3 s^{-1}	
k'_B	3 μM^{-1} s^{-1}	
k_A	50 μM^{-1} s^{-1}	
k_Y	100 μM^{-1} s^{-1}	
Sites methylated	K_m [mM]	V_m
0	$27 \cdot 10^{-4}$	0
1	$20 \cdot 10^{-3}$	0.25
2	$150 \cdot 10^{-3}$	0.5
3	$150 \cdot 10^{-2}$	0.75
4	60	1
Kinetic constants		
k_Z	30/[CheZ] s^{-1}	
K_R	0.099 μM	
K_B	2.5 μM	
γ_B	1.0 μM^{-1} s^{-1}	
γ_Y	0.1 μM^{-1} s^{-1}	
Total concentration [μM]		
A^T	5.3	
B^T	0.28	
R^T	0.08	
Y^T	9.7	
Z^T	3.8	
Hill curves		
H_m	1.2	
H_c	10.3	
K_c	3.1 μM	

CheR fluctuations

In the following, we will derive Eq. 1 from a simple model of binding and dissociation processes. The assumption that the CheR fluctuations originate in binding and dissociation processes is thereby motivated by the finding that the intracellular concentration of CheR is constant. This makes gene expression noise as origin of the fluctuations biologically unfeasible. For the form of Eq. 1, however, it does not matter which process is assumed to be the origin of the fluctuations. Equation 1 could also have been derived from a description of gene expression noise, with the parameter β depending on the degradation rate and steady-state concentration of CheR.

Here we consider the concentration of bound CheR (R), which increases in time when more free CheR (R_f) binds to the receptor complex (T), and decreases when bound CheR dissociates from the receptor. This can be written as

$$\frac{dR}{dt} = -k_{off}R + k_{on}R_f T.$$

Here, the dissociation is proportional only to the amount of bound CheR, whereas the dynamics of the binding process may depend on the concentration of free CheR and, for example, the receptor concentration. It is also possible to involve diffusion processes here, but as we will soon see, the exact form of the binding term is not crucial. What is important is that, at the steady state, the two processes (binding and dissociation) balance. Thus, at steady state holds

$$k_{off}R = k_{on}R_f T.$$

Now we assume that binding and dissociation are stochastic processes. Because the total concentration of CheR is at steady state, binding and dissociation balance, on average, but due to the stochasticity there can be deviations from the average concentration of bound CheR. In discrete terms, we can write the concentration of bound CheR at time t (R_t) depending upon R at time $t - \Delta t$ as

$$R_t = R_{t-\Delta t} + \text{binding} - \text{dissociation}.$$

Since we assume that the binding and dissociation processes are stochastic events, we model them by two random variables, χ_b and χ_d, respectively, with the following properties:

— Both random variables have the expectation $E(\chi_b) = E(\chi_d) = k_{off}R\,\Delta t$.
— The values χ_b and χ_d are uniformly distributed, although this assumption is not crucial. A Gaussian distribution would lead to similar fluctuations in CheR.

Thus, let χ_b and χ_d be uniformly distributed random variables in the interval $[0, k_{off}R\,2\Delta t]$. The difference $\chi(t) = \chi_b(t) - \chi_d(t)$ represents then, a new random variable in the interval $[k_{off}R\,-2\Delta t, k_{off}R\,2\Delta t]$. With this, we can write

$$R_t = R_{t-\Delta t} + \chi(t) = R_{t-\Delta t} + \beta\eta(t)\Delta t,$$

where we expressed $\chi(t)$ by the term $\beta\,\eta(t)\Delta t$, with η a random variable from the interval $[-1, 1]$, and the constant $\beta = 2k_{off}R$. This discrete equation corresponds, in the limit $\Delta \to 0$, to the continuous form of Eq. 1.

In Schulmeister et al. (23), FRET experiments were used to determine a number of kinetic parameters concerning binding and dissociation processes of proteins involved in the chemotaxis-signaling pathway. Here, k_{off} is given as 0.068 ± 0.008 s^{-1}. Furthermore, the measured parameters F and C indicate that, at steady state, approximately half of the CheR proteins are bound to receptors. With a total concentration of CheR 0.07 μM, we obtain, for β, a value of magnitude 10^{-3}.

Model parameters

The modeled bacteria move at the same speed as real bacteria, and also have the same average duration of CCW events. Their movement characteristics can therefore be compared to the behavior of real bacteria. The measured speed of *E. coli* during runs is ~30 $\pm$ 12 μm/s (38), with an average duration of CCW of 1 s (7). In our model, a single step in a given direction lasts 1/50 s, due to the choice of the time step for integration. Thus, the average duration of 1 s per run is obtained if runs take, on average, 50 consecutive steps. Using the dependence of the average run length on the CheR concentration (see Fig. 3), we find that the average run length comprises 50 steps for CheR levels at ~0.08 μM. Thus, for the low concentration values of CheR used in the model, the run duration also fits the experimental data. By adjusting the length of single steps to 0.6 μm, we achieve the characteristic speed.

The turning angles during the tumble can be fit by a Γ-distribution with shape parameter $\gamma = 4$, scale parameter $\beta = 18.32$, and location parameter $\mu = -4.6$ (39).

We thank M. Kollman, V. Sourjik, P. R. ten Wolde, W. Poon, and D. Frenkel for very useful discussions.

REFERENCES

1. Asakura, S., and H. Honda. 1984. Two-state model for bacterial chemoreceptor proteins. *J. Mol. Biol.* 176:349–367.
2. Kollmann, M., L. Løvdok, K. Bartholomé, J. Timmer, and V. Sourjik. 2005. Design principles of a bacterial signaling network. *Nature.* 438:504–507.
3. Bray, D., M. Levin, and K. Lipkow. 2007. The chemotactic behavior of computer-based surrogate bacteria. *Curr. Biol.* 17:R132–R134.
4. Levin, M., T. S. Shimizu, and D. Bray. 2002. Binding and diffusion of CheR molecules within a cluster of membrane receptors. *Biophys. J.* 82:1809–1817.
5. Lipkow, K., S. S. Andrews, and D. Bray. 2005. Diffusion of phosphorylated CheY through the cytoplasm of *Escherichia coli*. *J. Bacteriol.* 187:45–53.
6. Shimizu, T. S., S. V. Aksenov, and D. Bray. 2003. A spatially extended stochastic model of the bacterial chemotaxis signaling pathway. *J. Mol. Biol.* 329:291–309.
7. Berg, H., and D. Brown. 1972. Chemotaxis in *Escherichia coli* analyzed by three-dimensional tracking. *Nature*. 239:500–504.
8. Korobkova, E., T. Emonet, J. M. G. Vilar, T. S. Shimizu, and P. Cluzel. 2004. From molecular noise to behavioral variability in a single bacterium. *Nature*. 428:574–578.
9. Wu, M., J. W. Roberts, S. Kim, D. L. Koch, and M. P. DeLisa. 2006. Collective bacterial dynamics revealed using a three-dimensional population-scale defocused particle tracking technique. *Appl. Environ. Microbiol.* 72:4987–4994.
10. Metzler, R., and J. Klafter. 2000. The random walk's guide to anomalous diffusion: a fractional dynamics approach. *Phys. Rep.* 339:1–77.
11. Bartumeus, F., J. Catalan, U. L. Fulco, M. L. Lyra, and G. M. Viswanathan. 2002. Optimizing the encounter rate in biological interactions: Lévy versus Brownian strategies. *Phys. Rev. Lett.* 88:097901.
12. Bartumeus, F., M. G. E. da Luz, G. M. Viswanathan, and J. Catalan. 2005. Animal search strategies: a quantitative random-walk analysis. *Ecology.* 86:3078–3087.
13. Benichou, O., M. Coppey, M. Moreau, P. H. Suet, and R. Voituriez. 2005. A stochastic model for intermittent search strategies. *J. Phys. Condens. Matter.* 17:S4275–S4286.
14. Faustino, C. L., L. R. da Silva, M. G. E. da Luz, E. P. Raposo, and G. M. Viswanathan. 2007. Search dynamics at the edge of extinction: anomalous diffusion as a critical survival state. *Europhys. Lett.* 77:30002.
15. Viswanathan, G., V. Afanasyev, S. Buldyrev, E. Murphy, P. Prince, et al. 1996. Lévy flight search patterns of wandering albatrosses. *Nature.* 381:413–415.
16. Viswanathan, G. M., S. V. Buldyrev, S. Havlin, M. da Luz, E. Raposok, et al. 1999. Optimizing the success of random searches. *Nature.* 401:911–914.
17. Benhamou, S. 2007. How many animals really do the Lévy walk? *Ecology.* 88:1962–1969.
18. Reynolds, A. 2008. Deterministic walks with inverse-square power-law scaling are an emergent property of predators that use chemotaxis to locate randomly distributed prey. *Phys. Rev. E.* 78:011906.
19. Barkai, N., and S. Leibler. 1997. Robustness in simple biochemical networks. *Nature.* 387:913–917.
20. Le Novère, N., and T. S. Shimizu. 2001. StochSim: modeling of stochastic biomolecular processes. *Bioinformatics.* 6:575–576.
21. Levin, M. 2003. Noise in gene expression as the source of non-genetic individuality in the chemotactic response of *Escherichia coli*. *FEBS Lett.* 550:135–138.
22. Hansen, C. H., R. G. Endres, and N. S. Wingreen. 2008. Chemotaxis in *Escherichia coli*: a molecular model for robust precise adaptation. *PLOS Comp. Biol.* 4:14–27.
23. Schulmeister, S., M. Ruttorf, S. Thiem, D. Kentner, D. Lebiedz, et al. 2008. Protein exchange dynamics at chemoreceptor clusters in *Escherichia coli*. *Proc. Natl. Acad. Sci. USA.* 105:6403–6408.
24. Tu, Y., and G. Grinstein. 2005. How white nose generates power-law switching in bacterial flagellar motors. *Phys. Rev. Lett.* 94:208101.
25. Reference deleted in proof.
26. Sims, D. W., E. J. Southall, N. E. Humphries, G. C. Hays, C. J. A. Bradshaw, et al. 2008. Scaling laws of marine predator search behavior. *Nature.* 451:1098–1102.
27. Ramos-Fernández, G., J. L. Mateos, O. Miramontes, G. Cocho, H. Larralde, et al. 2004. Lévy walk patterns in the foraging movements of spider monkeys (*Ateles geoffroyi*). *Behav. Ecol. Sociobiol.* 55:223–230.
28. Brockmann, D., L. Hufnagel, and T. Geisel. 2005. The scaling laws of human travel. *Nature.* 439:462–465.
29. Brown, C. T., L. S. Liebovitch, and R. Glendon. 2007. Lévy flights in Dobe Ju/'Hoansi foraging patterns. *Hum. Ecol.* 35:129–138.
30. Edwards, A. M., R. A. Phillips, N. W. Watkins, M. P. Freeman, E. J. Murphy, et al. 2007. Revisiting Lévy flight search patterns of wandering albatrosses, bumblebees and deer. *Nature.* 449:1044–1048.
31. Sims, D. W., D. Righton, and J. W. Pitchford. 2007. Minimizing errors in identifying Lévy flight behavior of organisms. *J. Anim. Ecol.* 76:222–229.
32. White, E. P., B. J. Enquist, and J. L. Green. 2008. On estimating the exponent of power-law frequency distributions. *Ecology.* 89:905–912.
33. Boyer, D., G. Ramos-Fernández, O. Miramontes, G. Cocho, H. Larralde, et al. 2006. Scale-free foraging by primates emerges from their interaction with a complex environment. *Proc. R. Soc. Lond. B. Biol. Sci.* 273:1743–1750.
34. Mommer, M., and D. Lebiedz. 2007. Modeling subdiffusion using reaction diffusion systems. IWR preprint, University of Heidelberg available under http://www.ub.uni-heidelberg.de/archiv/7168.
35. Reference deleted in proof.
36. Emonet, T., and P. Cluzel. 2008. Relationship between cellular response and behavioral variability in bacterial chemotaxis. *Proc. Natl. Acad. Sci. USA.* 105:3304–3309.
37. Cluzel, P., M. Surette, and S. Leibler. 2000. An ultrasensitive bacterial motor revealed by monitoring signaling proteins in single cells. *Science.* 287:1652–1655.
38. Turner, L., W. S. Ryu, and H. C. Berg. 2000. Real-time imaging of fluorescent flagellar filaments. *J. Bacteriol.* 182:2793–2801.
39. Emonet, T., C. M. Macal, M. J. North, C. E. Wickersham, and P. Cluzel. 2005. AgentCell: a digital single-cell assay for bacterial chemotaxis. *Bioinformatics.* 21:2714–2721.